iScience

CellPress
OPEN ACCESS

Article

Transcriptome analysis of human hypertrophic cardiomyopathy reveals inhibited cardiac development pathways in children

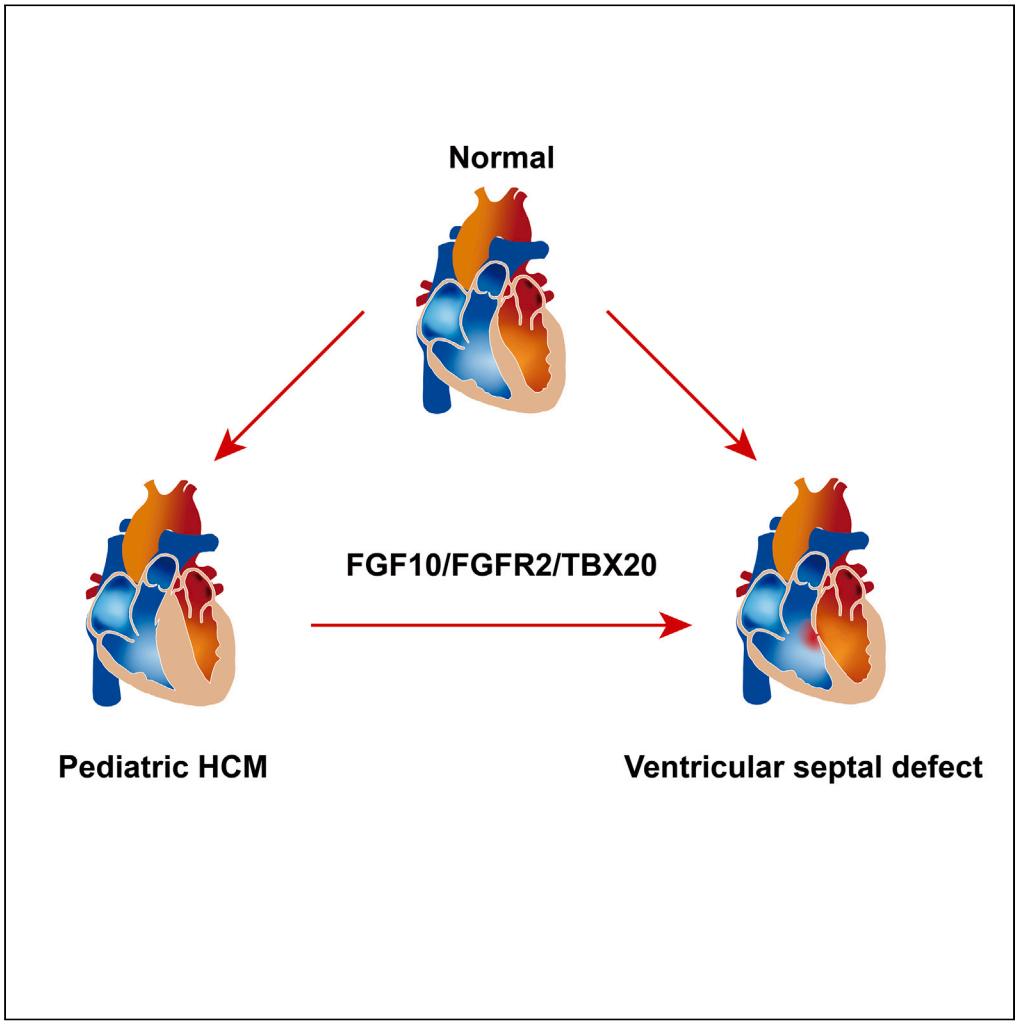

Shi Chen, Jingjing Hu, Yidan Xu, Jun Yan, Shoujun Li, Liang Chen, Jing Zhang

liang.chen9@hotmail.com (L.C.)
zhangjingfw@163.com (J.Z.)

Highlights

Adult HCM (A-HCM) and pediatric HCM (P-HCM) have distinct expression

The cardiac development related genes are downregulated in P-HCM

FGF10/FGFR2/TBX20 expression is negatively correlated with IVS thickness in P-HCM

Mitochondrial function related genes are specifically suppressed in A-HCM

Chen et al., iScience 27, 108642
January 19, 2024 © 2023
https://doi.org/10.1016/j.isci.2023.108642

iScience

CellPress
OPEN ACCESS

Article

Transcriptome analysis of human hypertrophic cardiomyopathy reveals inhibited cardiac development pathways in children

Shi Chen,[1,6] Jingjing Hu,[2,3,4,6] Yidan Xu,[5] Jun Yan,[1] Shoujun Li,[1] Liang Chen,[1,7,*] and Jing Zhang[1,5,7,8,*]

SUMMARY

The epidemiological, etiological, and clinical characteristics vary greatly between pediatric (P-HCM) and adult (A-HCM) hypertrophic cardiomyopathy (HCM) patients, and the understanding of the heterogeneous pathogenesis mechanisms is insufficient to date. In this study, we aimed to comprehensively assess the respective transcriptome signatures and uncover the essential differences in gene expression patterns among A-HCM and P-HCM. The transcriptome data of adults were collected from public data (GSE89714), and novel pediatric data were first obtained by RNA sequencing from 14 P-HCM and 9 infantile donor heart samples. Our study demonstrates the common signatures of myofilament or protein synthesis and calcium ion regulation pathways in HCM. Mitochondrial function is specifically dysregulated in A-HCM, whereas the inhibition of cardiac developing networks typifies P-HCM. These findings not only distinguish the transcriptome characteristics in children and adults with HCM but also reveal the potential mechanism of the higher incidence of septal defects in P-HCM patients.

INTRODUCTION

Pediatric hypertrophic cardiomyopathy (P-HCM) is one of the most common causes of sudden cardiac death (SCD) in the young population.[1,2] In contrast to adult cardiomyopathy, pediatric cardiomyopathies, including P-HCM, have significant differences in prevalence, etiology, and clinical features.[3] P-HCM was first included as a specific disease phenotype in the 2023 European Society of Cardiology (ESC) guidelines for the management of cardiomyopathies, and their unique clinical characteristics and management strategies have been described systematically.[4] The prevalence of P-HCM is approximately 0.029%, which is much lower than the prevalence of adult hypertrophic cardiomyopathy (A-HCM).[5] The etiology of P-HCM is more heterogeneous than that seen in adults and includes malformation syndromes, inborn errors of metabolism, and neuromuscular disorders.[6] P-HCM is characterized by hypertrophy of the myocardium in the interventricular septum (IVS) and left ventricular free wall and myocardial disarray with mild fibrosis, which are inconsistent with the characteristics of A-HCM.[7] The long-term prognosis of P-HCM patients is poor, as they have a higher risk of developing adverse heart failure and at least a 50% higher risk of SCD than A-HCM patients.[8] In summary, although the incidence of P-HCM is lower than that of A-HCM, the clinical characteristics are more varied, and the prognosis is worse.

It is well known that the clinical phenotypes of P-HCM and A-HCM differ. Due to the higher heterogeneity and worse prognosis in P-HCM, it is necessary to understand its specific pathogenesis and the mechanisms that differ between P-HCM and A-HCM. Nevertheless, studies revealing the underlying diversity are lacking, especially at the transcriptome level. Prior RNA sequencing (RNA-seq) studies on HCM are limited and mainly enrolled adult patients but not infants and young patients.[9–12] The patient-specific networks in A-HCM could vary in complexity based on their findings.[12] Therefore, based on reasonable assumptions, the heterogeneity of gene expression patterns could be greater among infantile and adult HCM patients.

Thus, we performed RNA-seq analysis for hypertrophied and normal myocardium from P-HCM patients who underwent septum myectomy surgery and healthy pediatric donors for the first time. In this work, we aimed to describe the transcriptomic signatures of P-HCM, explore its unique pathogenic mechanism that differs from that of A-HCM, and uncover the correlation between its specific clinical characteristics and gene expression patterns. To avoid transcriptome differences caused by ethnic heterogeneity, a public dataset including Chinese individuals

[1]State Key Laboratory of Cardiovascular Disease, Fuwai Hospital, National Center for Cardiovascular Diseases, Chinese Academy of Medical Sciences and Peking Union Medical College, Beijing, China
[2]Key Laboratory of Public Health Safety, Ministry of Education, Fudan University; Shanghai, China
[3]Shanghai Pinnacles Medical Technology Co., Ltd, Shanghai 200126, China
[4]Department of Epidemiology, School of Public Health, Fudan University, Shanghai, China
[5]Department of Cardiac Surgery, Fuwai Hospital Chinese Academy of Medical Sciences, Shenzhen, Shenzhen, China
[6]These authors contributed equally
[7]These authors contribute equally
[8]Lead contact
*Correspondence: liang.chen9@hotmail.com (L.C.), zhangjingfw@163.com (J.Z.)
https://doi.org/10.1016/j.isci.2023.108642

with RNA-seq data from myocardium samples was utilized, and A-HCM patients and healthy adults were compared. Comprehensive bioinformatics analysis strategies, including weighted gene coexpression network analysis (WGCNA), differentially expressed gene (DEG) analysis, and Reactome pathway analysis, were applied to identify the potential biological functions and modules related to HCM pathogenesis. In addition, single-cell deconvolution analysis was used to identify the key cell type involved in the P-HCM pathophysiological process. qRT−PCR and western blot methods were also applied to validate gene expression at the RNA and protein levels.

RESULTS

Transcriptomic profiles and WGCNA network analysis

The gene expression matrices of hypertrophic cardiomyopathy (HCM) patients and healthy donors at a younger or older age were obtained from our original RNA-seq data and public data (GSE89714) after data processing (Figure 1A). The clinical characteristics of P-HCM and P-Normal are listed in Table 1. The details of the pathogenic mutations in P-HCM patients are listed in Table 2. The gene mutations were complicated in P-HCM patients and included *PTPN11*, *RAF1*, and *NOTCH1* mutations in addition to common A-HCM mutations, such as *MYBPC3* and *MYH6*. The typical preoperative transesophageal echocardiogram and histopathological characteristics of P-HCM patients are presented in Figures 1B and 1C.

The WGCNA was performed by using combined gene expression matrices from our study (P-HCM) and public data (A-HCM), and the coexpression network was constructed to identify the key biological function modules related to the pathogenesis of pediatric or adult HCM. A total of nine independent modules, except M5, were identified based on average hierarchical clustering and dynamic tree clipping, and the M5 module was composed of all the genes that were not distributed to any other modules (Figures 1D–1F). The gene lists of all the modules are shown in Data S1. The results of module-trait relationship analysis showed that M9 ($r = -0.61$, $p = 2.4*10^{-4}$) and M10 ($r = 0.42$, $p = 0.017$) were strongly correlated with A-HCM. In addition, for the infantile patients, M9 ($r = 0.56$, $p = 0.00091$) and M10 ($r = 0.49$, $p = 0.004$) were also strongly correlated with the P-HCM phenotype (Figure 1E). These results suggest that both M9 and M10 were common functional modules in both adult and pediatric HCM patients. However, M2 ($r = 0.53$, $p = 1.8*10^{-3}$) and M8 ($r = 0.5$, $p = 3.2*10^{-3}$), which were relatively positively correlated with P-Normal, were also negatively correlated with P-HCM. M2 and M8 were both negatively correlated with A-HCM and A-Normal (Figure 1E). The heatmap also showed that M2 and M8 were differentially expressed between P-HCM and P-Normal, which suggests that M2 and M8 could be the potential specific key modules related to P-HCM pathogenesis (Figure 1H). To further explore the specific biological functions of these modules, GO analysis, including cell component (CC), biological process (BP) and molecular function (MF) categories, was applied. As a result, M9 and M10 were both enriched in protein folding and synthesis, and M8 was enriched in the regulation of mRNA processing and RNA splicing (Figures S1–S3). Interestingly, the genes in the M2 module, which were downregulated in the P-HCM group, were mainly associated with cardiac chamber morphogenesis and muscle tissue development (Figure S4).

DEGs and GO enrichment analysis

The characteristics of the RNA-seq data from the two datasets were visualized by principal component analysis (PCA) plots (Figure 2A). As expected, there were obvious heterogeneous transcriptomics features between infants and adults, and the gene expression patterns significantly differed between P-HCM and P-Normal and between A-HCM and A-Normal. The heterogeneity within HCM patients was more obvious among the P-HCM group than among the A-HCM group, which could be caused by the heterogeneous genetic background in P-HCM patients (Figure 2A). The DEGs of each group are presented in a Venn diagram (Figure 2B). There were 488 and 501 up- and downregulated genes in P-HCM compared with P-Normal, respectively. A total of 1384 genes were upregulated and 1005 genes were downregulated in A-HCM compared with A-Normal. There were 93 suppressed DEGs and 184 activated DEGs in both A-HCM and P-HCM patients. The DEGs of the various phenotypes are listed in Data S2. Volcano plots of all DEGs (Figures 2C and 2D) and cluster heatmaps of the top 50 DEGs were generated to compare the gene expression profiles with the adjusted p values ($-\log_{10}$) based on the two datasets from children and adults (Figures S5 and S6). The results showed that the DEG expression fold changes between A-HCM and A-Normal were greater than those between P-HCM and P-Normal.

GO term enrichment analysis was performed to identify the functional pathways in which DEGs were subsequently significantly enriched. In the A-HCM group, the upregulated DEGs were enriched in extracellular matrix (ECM) organization, actin filament organization, cellular response to TGF-β stimulus and regulation of cytosolic calcium ion concentration pathways. Moreover, the expression levels of genes involved in energy metabolism, oxidative phosphorylation, cellular respiration and mitochondrial ATP synthesis pathways were suppressed in the A-HCM transcriptome (Figure 2E), but these effects were not significant in the P-HCM transcriptome (Figure S7). In P-HCM, there was also enrichment for the activation of actin filament organization, cellular calcium ion homeostasis, cell-substrate adhesion, and regulation of vasculature development. Nonetheless, the enriched pathways of the downregulated genes in P-HCM pathologies were quite different, and the genes in heart structural development-related pathways, including cardiac chamber development, cardiac septum development and heart morphogenesis, were apparently inhibited (Figure 2F).

Reactome pathway analysis

Reactome is one of the most widely used biological pathway knowledge bases and is integrated into the web Cytoscape for pathway analysis. The results of Reactome analysis, which were consistent with those of the GO enrichment analysis, suggested that the activated pathways in A-HCM (vs. A-Normal) were mainly annotated by ECM organization, protein metabolism, muscle contraction, and apoptosis (Figures 3A, 3C,

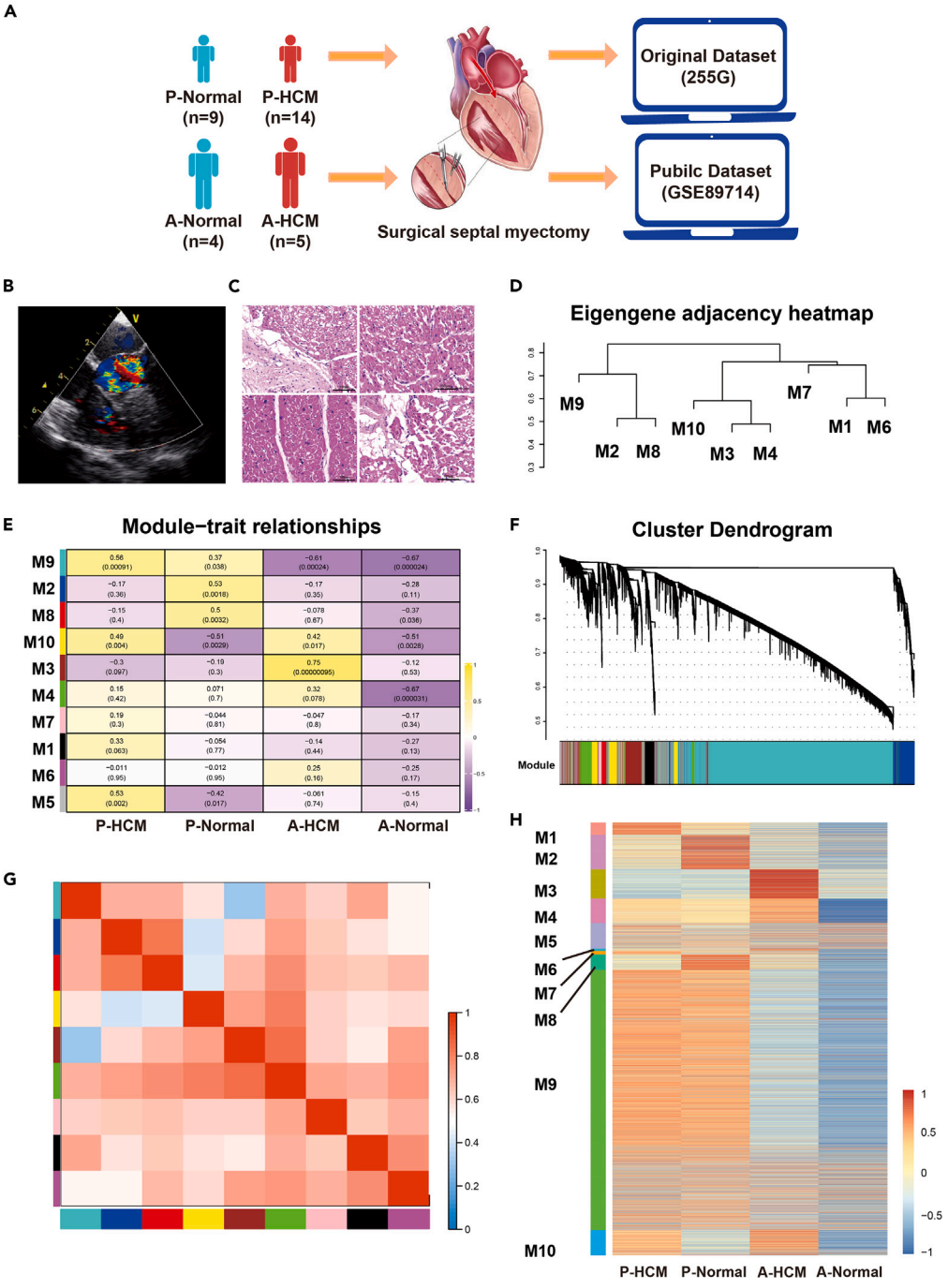

Figure 1. The study design and weighted correlation network analysis (WGCNA) identified the specific functional module in HCM

(A) The flowchart of our study.

(B) The representative preoperative transesophageal echocardiogram of a P-HCM patient.

(C) The representative histopathological characteristics of P-HCM patients.

(D) Hierarchical clustering of the defined modules. The dendrogram indicated the distance/similarity of modules.

(E) Heatmap of the correlation between gene modules and clinical phenotype.

(F) The WGCNA cluster dendrogram defined all detected genes into 9 modules. See also Figures S1–S4.

(G) Module-trait heatmap of the relationships in the module network.

(H) The specific gene expression levels of genes in individual modules among different subgroups of patients.

Table 1. Baseline characteristics of P-HCM patients enrolled for RNA-seq

	P-HCM (n = 14)	P-Normal (n = 9)	p value
Demographic			
Male (%)	8 (57.14)	6 (66.67)	1.000
Age at diagnosis (years)	0.91 ± 1.35	NA	NA
Age at operation (years)	3.42 ± 3.06	NA	NA
Imaging			
LA (mm)	31.79 ± 9.67	20.33 ± 8.76	0.009
IVS (mm)	17.18 ± 7.54	4.89 ± 0.33	<0.001
LVEDD (mm)	29.29 ± 7.29	28.67 ± 9.10	0.858
LVPW (mm)	10.94 ± 6.43	4.56 ± 0.53	0.003
LVEF (%)	72.30 ± 8.42	70.11 ± 5.23	0.494
SAM	12 (85.71)	0 (0.00)	<0.001
LVOTPG (mmHg)	80.92 ± 30.69	NA	NA
RVEDD (mm)	13.79 ± 3.24	12.67 ± 2.29	0.450

P-HCM, pediatric hypertrophic cardiomyopathy; LA, left atrium; IVS, interventricular septum; LVEDD, left ventricular end-diastolic diameter; LVPW, left ventricular posterior wall; LVEF, left ventricular ejection fraction; SAM, systolic anterior motion of mitral; LVOTPG, left ventricular outflow tract pressure gradient; RVEDD, right ventricular end-diastolic diameter.

and 3E). The energy synthesis-related pathways were inhibited in contrast (Figure 3G). In P-HCM, the upregulated pathways were also related to muscle contraction and protein metabolism, which is relatively similar to the A-HCM gene expression pattern (Figures 3B, 3D, and 3F). Nevertheless, the role of FGFR signaling pathways in disease, especially that of FGFR2, was specifically downregulated in P-HCM (Figures 3D and 3H).

Regulation network and gene expression correlation analyses

The annotation of upregulated genes in P-HCM revealed significant enrichment of well-characterized HCM pathologies, including actin filament organization, cellular calcium ion homeostasis, and positive regulation of secretion (Figure 4A). In contrast, the downregulated genes in P-HCM were enriched in pathways associated with ventricular septal dysplasia, including cardiac chamber development, cardiac septum

Table 2. Identified gene mutations in P-HCM patients enrolled for RNA-seq

No. ID	Gene	cDNA change	Genotype	AA change	Pathogenicity
P1	MYH6	c.2836G>A	Hetero	p.E946K	LP
	MYH6	c.2630A>C	Hetero	p.E877T	VUS
	MYH6	c.2629G>A	Hetero	p.E877T	P
P2	MYBPC3	c.3719T>C	Hetero	p.I1240T	VUS
P3	TRPM4	c.3237delT	Hetero	–	LP
P4	MYBPC3	c.3148G>A	Hetero	p.E1050K	VUS
P5	TNNT2	c.248A>G	Hetero	p.N83S	VUS
P6	TTN	c.18493G>A	Hetero	p.V6165M	VUS
P7	RAF1	c.770C>T	Hetero	p.S257L	P
P8	RAF1	c.788T>G	Hetero	p.V263G	LP
P9	TTN	c.92979A>T	Hetero	p.K30993N	VUS
P10	PTPN11	c.1517A>C	Hetero	p.Gln506Pro	P
P11	PTPN11	c.1528C>G	Hetero	p.Gln510Glu	P
P12	LZTR1	c.2406 + 1G>C	Hetero	N/A	VUS
	LZTR1	c.1385T>C	Hetero	p.I462T	VUS
P13	RAF1	c.781C>T	Hetero	p.P261S	P
P14	NOTCH1	c.3274C>T	Hetero	p.Leu1092Phe	VUS

P-HCM, pediatric hypertrophic cardiomyopathy; AA, amino acid; LP, likely pathogenic; P, Pathogenic; VUS, Variant of Uncertain Significance.

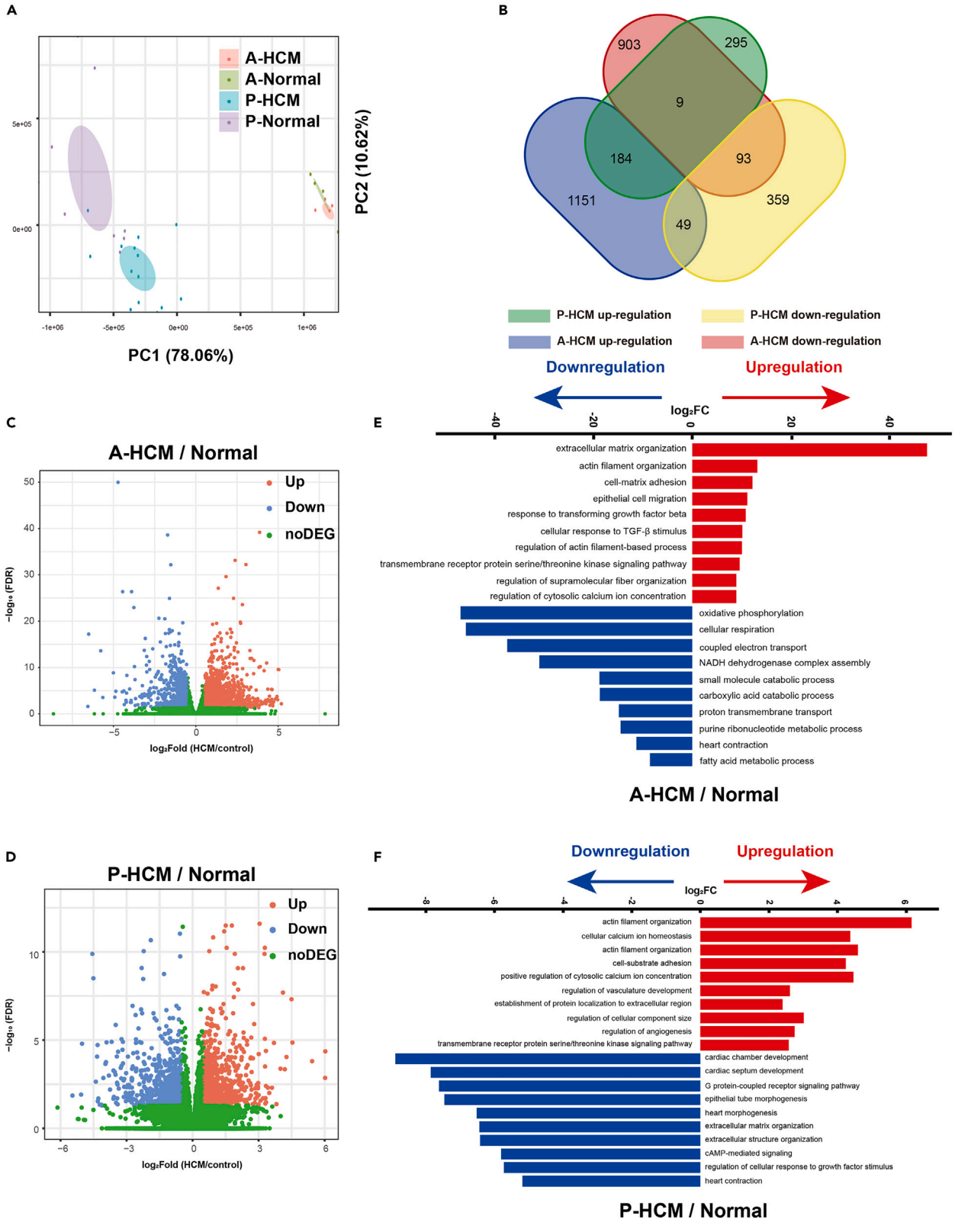
A
A-HCM
A-Normal
P-HCM
P-Normal
PC1 (78.06%)
PC2 (10.62%)
B
903
295
9
184
93
1151
359
49
P-HCM up-regulation
P-HCM down-regulation
A-HCM up-regulation
A-HCM down-regulation
C
A-HCM / Normal
Up
Down
noDEG
log₂Fold (HCM/control)
D
P-HCM / Normal
E
Downregulation
Upregulation
log₂FC
extracellular matrix organization
actin filament organization
cell-matrix adhesion
epithelial cell migration
response to transforming growth factor beta
cellular response to TGF-β stimulus
regulation of actin filament-based process
transmembrane receptor protein serine/threonine kinase signaling pathway
regulation of supramolecular fiber organization
regulation of cytosolic calcium ion concentration
oxidative phosphorylation
cellular respiration
coupled electron transport
NADH dehydrogenase complex assembly
small molecule catabolic process
carboxylic acid catabolic process
proton transmembrane transport
purine ribonucleotide metabolic process
heart contraction
fatty acid metabolic process
A-HCM / Normal
F
actin filament organization
cellular calcium ion homeostasis
actin filament organization
cell-substrate adhesion
positive regulation of cytosolic calcium ion concentration
regulation of vasculature development
establishment of protein localization to extracellular region
regulation of cellular component size
regulation of angiogenesis
transmembrane receptor protein serine/threonine kinase signaling pathway
cardiac chamber development
cardiac septum development
G protein-coupled receptor signaling pathway
epithelial tube morphogenesis
heart morphogenesis
extracellular matrix organization
extracellular structure organization
cAMP-mediated signaling
regulation of cellular response to growth factor stimulus
heart contraction
P-HCM / Normal

Figure 2. Differentially expressed gene (DEG) and pathway analyses

(A) The Venn diagram shows the numbers of up- and downregulated genes in P-HCM and A-HCM separately.

(B) The principal component analysis showed that the transcriptome characteristics varied significantly among children and adults.

(C) Volcano plot of A-HCM and A-Normal. See also Figure S5.

(D) Volcano plot of P-HCM and A-Normal. See also Figure S6.

(E) The activated and inhibited pathways in A-HCM compared with A-Normal.

(F) The activated and inhibited pathways in P-HCM compared with P-Normal. See also Figure S7.

development, and epithelial tube morphogenesis. The genes involved in these pathologies that were dysregulated in P-HCM are illustrated in Figure 4B.

The gene expression regulation network of these three inhibited pathways in P-HCM was established, and FGFR2, FGF10, TGFBR3, and TBX20 were characterized as the hub genes of this network (Figure 5A). To further illustrate the co-expression trends among FGFR2, FGF10, TGFBR3, and TBX20, we performed Spearman correlation analysis. The results suggested that all of these genes were highly positively correlated (p value <0.001) (Figure 5B). In addition, the expression levels of these genes were negatively correlated with the thickness of the IVS, which was the most typical histopathological change in hypertrophic obstructive cardiomyopathy (Figure 5C). The gene expression and protein levels of these genes in P-HCM were all considerably lower than those in P-Normal (Figures 5D and 5E).

Cell type abundance and cell interactions

CIBERSORTx was used to identify the differences in cell type abundance between normal and HCM myocardium. The marker genes that were used to define the cell types are listed in Data S3. The ratios of major cell types in each human sample from the P-HCM, P-Normal, A-HCM and A-Normal groups are presented in Figure 6A. The ratio of cardiomyocytes (CMs) was significantly lower in the A-HCM group than in the A-Normal group (Figure 6B). This could be explained by the larger size of hypertrophied CMs and the increase in CM apoptosis, leading to a decrease in the number of CMs in a certain volume of myocardial tissue. Correspondingly, the abundance of smooth muscle cells, fibroblasts (FBs), and endothelium apparently increased (Figure 6B), which could be caused by the activation of angiogenesis and the ECM synthesis process. Inflammatory cells, including macrophages and lymphocytes, were not significantly recruited in the A-HCM group.

In P-HCM tissue samples, the abundance of CMs was close to that in the P-Normal group (58.92 $\pm$ 3.29% vs. 60.74 $\pm$ 2.78%, $p = 0.187$), while the infiltration of lymphocytes and pericytes was increased. The percentages of fibroblasts and endothelium were decreased in P-HCM, and the opposite trend was observed in A-HCM pathologies (Figure 6C). In addition, the expression levels of hub genes in the heart structural development regulation networks, including *FGFR2* (correlation coefficient = 0.853, $p < 0.001$) and *FGF10* (correlation coefficient = 0.493, $p = 0.018$), were positively correlated with the abundance of fibroblasts in pediatric samples. The expression level of *TBX20* (correlation coefficient = 0.483, $p = 0.021$), another hub gene in this network, was correlated with the CM percentage (Figure 6D). The results indicated that FBs and CMs could have potential cell interactions in P-HCM pathologies.

DISCUSSION

Common dysregulated transcriptome signatures in HCM

In our study, we first profiled the transcriptome of young children with HCM and compared the characteristics of pediatric and adult HCM patients at the gene expression level. The imaging and histopathological characteristics of P-HCM in our study are typical. The etiology and pathogenic mutations were heterogeneous in P-HCM patients, which is consistent with previous large pediatric cardiomyopathy cohort studies.[3] The fold-changes of a total of 338 DEGs trended in the same direction in infant and adult HCM patients, and these DEGs only accounted for a relatively low proportion of the detected genes. Not surprisingly, our WGCNA and DEG analysis confirmed that metabolic processes, including protein synthesis, actin filament organization, and regulation of cytosolic calcium ion concentration, were activated in both A-HCM and P-HCM. The pathological hypertrophy of CMs could activate the fetal gene program and increase the cell size, and therefore, the metabolism process of peptide synthesis and protein folding would be upregulated.[13] Additionally, it is commonly recognized that mutations of the genes encoding myofilament proteins and the abnormality of cardiac myofilament hypertrophy are the key pathogenic and pathological characteristics of HCM.[14] Thus, the dysregulation of genes in actin filament organization pathways, including *MYO1D*, *F2R*, *STC1*, and *JAK2*, is clear. Additionally, an increase in myofilament Ca^{2+} sensitivity is commonly observed in HCM, and dysregulation of the cytosolic calcium ion concentration has been shown to be one of the main causes of afterdepolarization and reentry arrhythmias.[15,16] Our results emphasize that impaired Ca^{2+} homeostasis would also affect electrophysiological activities in P-HCM, as in older patients.

Energetic metabolism differences in A-HCM and P-HCM

The dynamic balance of ATP synthesis and consumption is widely adaptive in the physiological state of the heart to maintain normal systolic function and electromyographic signal conduction under various conditions.[17] However, abnormalities in cardiac energetics have been found even at the early stage of HCM.[18] The results in our study suggest that genes involved in the pathways of the tricarboxylic acid cycle, respiratory electron transport, and especially fatty acid metabolism are downregulated in A-HCM, including *ACSL3*, *SLC27A4*, *NDUFAB1*, and *ECH1*. Our findings are consistent with previous studies suggesting that A-HCM was associated with cardiac bioenergetic reduction and the alteration of energy metabolic substrates. In summary, the perturbed energy metabolic signaling and mitochondrial dysfunction are common pathogenic mechanisms in A-HCM specifically.[17–19]

A

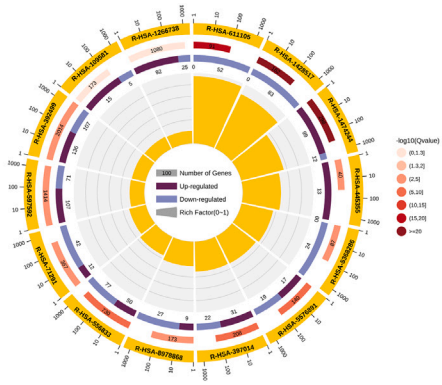

B

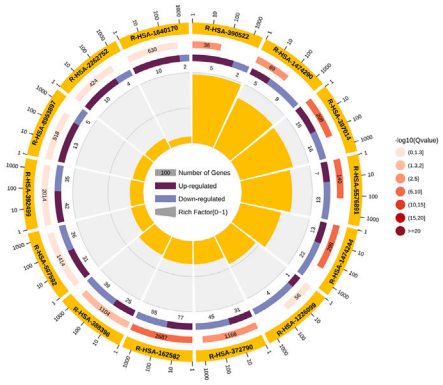

C

ID	Term (Up/Down in A-HCM)
R-HSA-1474244	Extracellular matrix organization
R-HSA-397014	Muscle contraction
R-HSA-392499	Metabolism of proteins
R-HSA-109581	Apoptosis
R-HSA-611105	Respiratory electron transport
R-HSA-5368286	Mitochondrial translation initiation
R-HSA-8978868	Fatty acid metabolism
R-HSA-5576891	Cardiac conduction

D

ID	Term (Up/Down in P-HCM)
R-HSA-390522	Striated Muscle Contraction
R-HSA-392499	Metabolism of proteins
R-HSA-2262752	Cellular responses to external stimuli
R-HSA-1640170	Cell Cycle
R-HSA-1474290	Collagen formation
R-HSA-1474244	Extracellular matrix organization
R-HSA-1226099	Signaling by FGFR in disease
R-HSA-372790	Signaling by GPCR

E

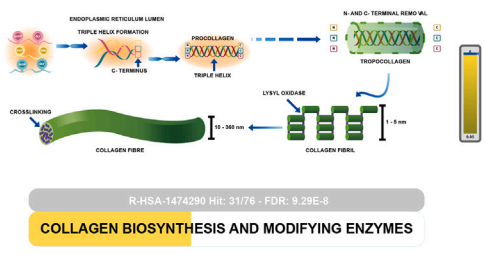

F

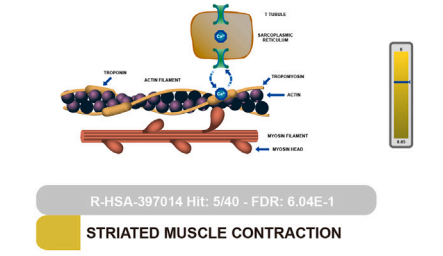

G

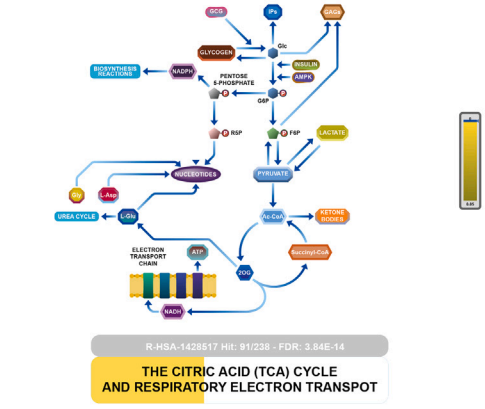

H

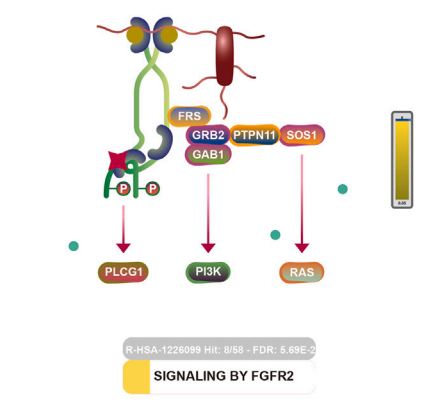

Figure 3. Reactome pathway analysis in A-HCM and P-HCM

(A) The up- and downregulated Reactome pathways in A-HCM.

(B) The up- and downregulated Reactome pathways in P-HCM.

(C) Specific lists of differentially expressed terms in A-HCM.

(D) Specific lists of differentially expressed terms in P-HCM.

(E) Schematic diagram of activated collagen biosynthesis and modifying enzyme pathways in A-HCM.

(F) Schematic diagram of the activated striated muscle contraction pathway in P-HCM.

(G) Schematic diagram of the inhibition of the citric acid cycle and respiratory electron transport pathway in A-HCM.

(H) Schematic diagram of the inhibition of the FGFR2 signaling pathway in P-HCM.

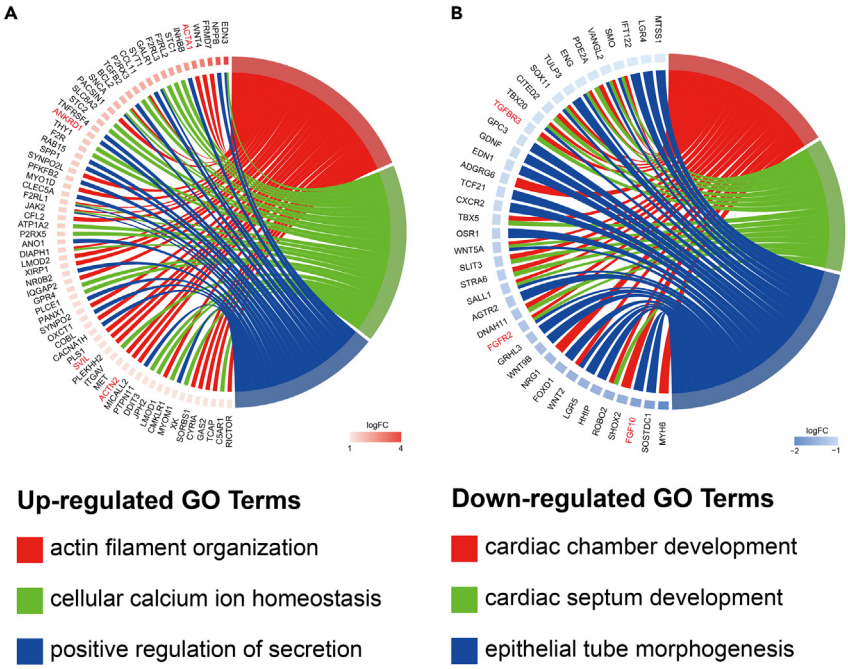

Figure 4. Regulation networks and hub gene expression patterns in P-HCM

(A) The circus plots of upregulated specific gene networks in P-HCM.

(B) The circus plots of downregulated specific gene networks in P-HCM.

However, another important finding is that similar trends of upregulation of these genes were not found among P-HCM patients. It has been well recognized that the swift transition of energy metabolism patterns from carbohydrate to lipid metabolism occurs rapidly in CM maturation after birth. The degradation of fatty acids in CMs was dramatically increased to meet the considerably higher energy demand for contractile function.[20,21] In addition, to adapt to the increased cardiac workload during the postnatal period, heart mass is increased by CM hyperplasia and hypertrophy.[22] In other words, the physiological hypertrophy of CMs was accompanied by increased fatty acid metabolism and energy synthesis in infants. In our study, the expression levels of genes, including *NDUFAB1*, *UQCR10*, *COX5A*, *PLIN5*, and *ACAT1*, in oxidative phosphorylation and fatty acid metabolism pathways were neither up- nor downregulated significantly during the pathological CM hypertrophy process in P-HCM. Thus, the specific network regulation of energy metabolism patterns in P-HCM needs further research in the future.

Cardiac development pathways were specifically suppressed in P-HCM

The balanced expression of genes in the cardiac chamber and septum development pathways is essential during the process of cardiac morphogenesis. It has been found that *de novo* mutations of specific genes in these pathways, including *FGF10, FGFR2, and TBX20*, are associated with congenital cardiac dysplasia occurrence, especially ventricular septal defect (VSD), in human cohort studies.[23–28] Additionally, gene-edited *FGF10* and *FGFR2* mutant mouse models developed outflow tract and ventricular hypoplasia.[25,28] *TBX20* is necessary and sufficient to promote CM proliferation. *TBX20* loss of function reduces CM abundance and affects cardiac development *in vivo*.[26,28] However, the association between the expression levels of these genes and P-HCM has not been reported.

In clinical studies, the potential relationship between P-HCM and the VSD phenotype has long been underrecognized. P-HCM and VSD are two independent congenital malformations with opposite pathological muscular features. The IVS thickness and the cell size of CMs were increased in P-HCM, while the IVS and the CMs were lost in VSD. A few pediatric case reports with combined HCM and VSD revealed the possibility of the coexistence of these two phenotypes in past decades.[29–31] Furthermore, the latest results from a multicenter European cohort study of infantile HCM indicated that the incidence of VSD in P-HCM patients (12%) is approximately 40 times greater than that of the general newborn population (0.3%).[3]

In our study, the M2 module represented by cardiac morphogenesis was downregulated in P-HCM based on WGCNA. The DEG results suggested that the expression of the specific genes in the *FGF10/FGFR2/TBX20* regulatory network with the biological function of septum development was inhibited in P-HCM, and the FGFR2 signaling pathways in disease were also suppressed. The expression levels of *FGF10/FGFR2/TBX20* were significantly negatively correlated with IVS thickness in infantile HCM. Deconvolution analysis showed that *FGF10/FGFR2* expression was correlated with FB abundance, while *TBX20* expression was correlated with CM abundance. Combined with the above results, these results indicate that the potential cell interaction between the FBs and CMs achieved by *the FGF10/FGFR2/TBX20* network could link

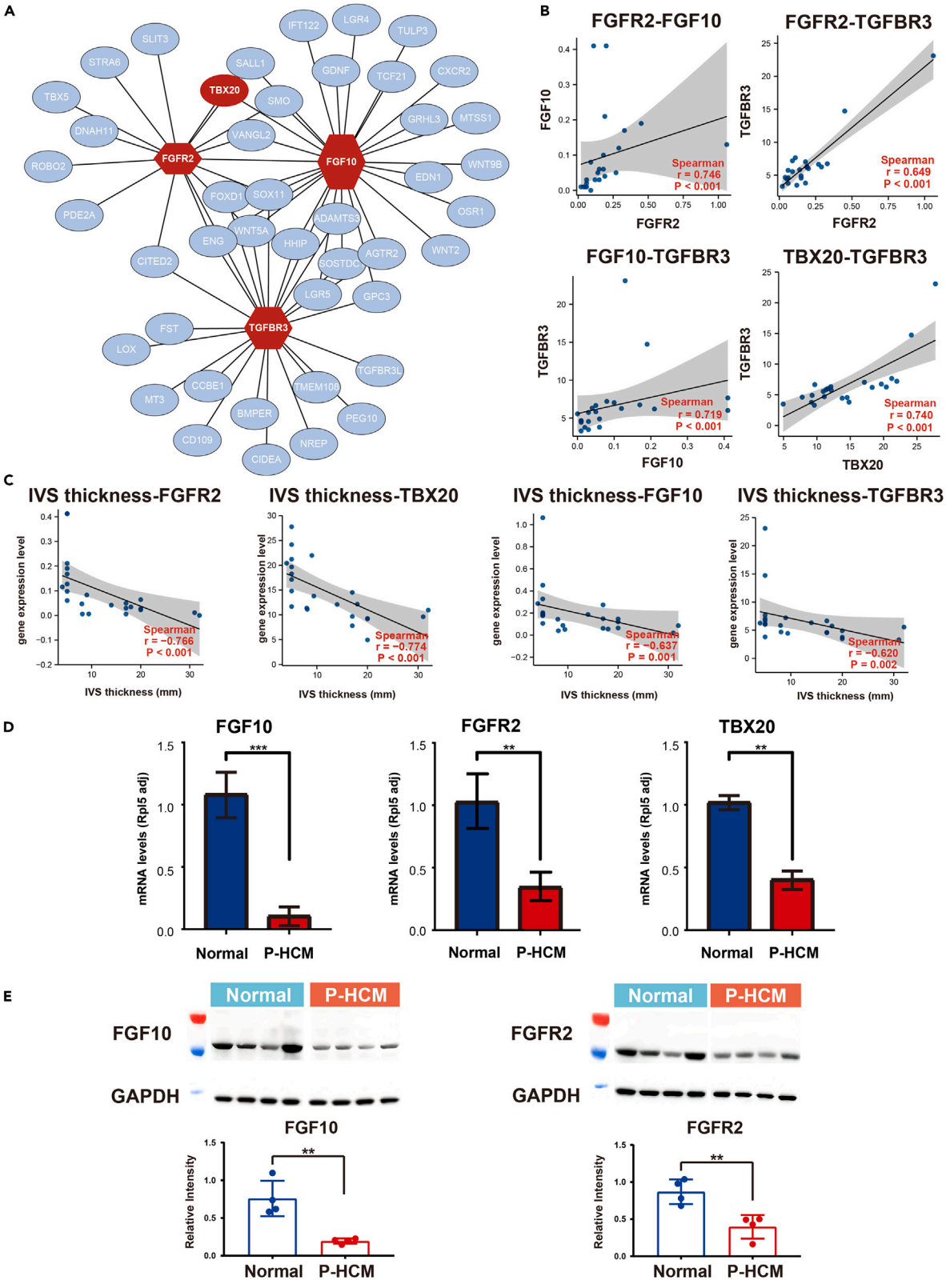
A
IFT122
LGR4
TULP3
SLIT3
STRA6
SALL1
GDNF
TCF21
CXCR2
TBX20
TBX5
SMO
GRHL3
MTSS1
DNAH11
VANGL2
FGFR2
FGF10
ROBO2
WNT9B
EDN1
FOXD1
SOX11
PDE2A
ADAMTS3
OSR1
ENG
WNT5A
HHIP
AGTR2
WNT2
CITED2
SOSTDC
LGR5
GPC3
TGFBR3
FST
LOX
TGFBR3L
CCBE1
TMEM100
MT3
BMPER
PEG10
CD109
NREP
CIDEA
B
FGFR2-FGF10
FGF10
FGFR2
Spearman
r = 0.746
P < 0.001
FGFR2-TGFBR3
TGFBR3
FGFR2
Spearman
r = 0.649
P < 0.001
FGF10-TGFBR3
TGFBR3
FGF10
Spearman
r = 0.719
P < 0.001
TBX20-TGFBR3
TGFBR3
TBX20
Spearman
r = 0.740
P < 0.001
C
IVS thickness-FGFR2
gene expression level
IVS thickness (mm)
Spearman
r = −0.766
P < 0.001
IVS thickness-TBX20
gene expression level
IVS thickness (mm)
Spearman
r = −0.774
P < 0.001
IVS thickness-FGF10
gene expression level
IVS thickness (mm)
Spearman
r = −0.637
P = 0.001
IVS thickness-TGFBR3
gene expression level
IVS thickness (mm)
Spearman
r = −0.620
P = 0.002
D
FGF10
mRNA levels (Rpl5 adj)
***
Normal
P-HCM
FGFR2
mRNA levels (Rpl5 adj)
**
Normal
P-HCM
TBX20
mRNA levels (Rpl5 adj)
**
Normal
P-HCM
E
Normal
P-HCM
FGF10
GAPDH
FGF10
Relative Intensity
**
Normal
P-HCM
Normal
P-HCM
FGFR2
GAPDH
FGFR2
Relative Intensity
**
Normal
P-HCM

Figure 5. The expression of hub genes in the cardiac development pathways

(A) The specific *FGF10/FGFR2/TBX20* regulatory network of cardiac development function. The hub genes were highlighted in red and their targets were shown.

(B) Spearman correlation analysis between *FGF10/FGFR2/TBX20* and *TGFBR3* on our dataset, each dot accounted for a sample.

(C) Spearman correlation analysis between interventricular septal thickness and specific gene expression levels in the P-HCM and P-Normal groups.

(D) Transcriptional profiling of hub genes in the network using qRT−PCR in P-HCM patients and young healthy donors. The samples used in the experiment were derived from interventricular septum. The relative expression was normalized by GAPDH. The results are presented as the mean ± SEM. N = 4 in both normal and P-HCM group. Differences between groups (p value) were calculated by unpaired two-tailed *t*-test. *p < 0.05; **p < 0.01; ***p < 0.001.

(E) Ratio of FGF10 and FGFR2 in interventricular septum from P-HCM patients and young healthy donors measured by Western blot assays (n = 4 patients per group). The relative expression was normalized by GAPDH. The results are presented as the mean ± SEM. N = 4 in both normal and P-HCM group. Differences between groups (p value) were calculated by unpaired two-tailed *t*-test. *p < 0.05; **p < 0.01; ***p < 0.001.

the VSD and HCM phenotypes. In this study, we propose a novel hypothesis, and further exploration intends to reveal the deeper comprehensive mechanics of the strong connection between VSD and HCM in newborns in the future.

This is the first transcriptome analysis study of A-HCM and P-HCM human heart tissue, which are rare and valuable biological samples. The transcriptome signatures of pediatric and adult HCM patients shared the similarities of actin filament organization, calcium ion regulation, and protein synthesis pathway activation and also differed in some other critical functions. Our results demonstrate mitochondrial dysfunction in A-HCM patients, which suggests that specific therapies targeting energy metabolism are important. Additionally, this study first revealed the potential mechanism of the newly discovered clinical phenomenon that the dysregulation of the *FGF10/FGFR2/TBX20* network in CM and FB cell interactions would lead to a significantly higher VSD incidence in P-HCM patients.

Limitations of the study

The A-HCM transcriptome data were obtained from a public dataset. The clinical characteristics and genetic background of these patients were unavailable; therefore, some correlation or comparison could not be performed with pediatric patients in our study from clinical aspects. The heart samples in both the P-HCM and A-HCM groups were collected from hypertrophied IVS myocardium, and the transcriptome pattern in other parts of the heart could be different. The findings from this study are based on cross-sectional study, however, the mechanistic validation still requires further cell experiments and/or transgenic animal model.

STAR★METHODS

Detailed methods are provided in the online version of this paper and include the following:

- KEY RESOURCES TABLE
- RESOURCE AVAILABILITY
  - Lead contact
  - Materials availability
  - Data and code availability
- EXPERIMENTAL MODEL AND STUDY PARTICIPANT DETAILS
  - Human subjects
- METHOD DETAILS
  - Library preparation and RNA sequencing
  - Quantitative real-time PCR (qRT−PCR)
  - Western blot
- QUANTIFICATION AND STATISTICAL ANALYSIS
  - Transcriptomics data analysis
  - DEGs and gene ontology (GO) analysis
  - Reactome pathway analysis
  - Deconvolution analysis
  - Statistical analysis

SUPPLEMENTAL INFORMATION

Supplemental information can be found online at https://doi.org/10.1016/j.isci.2023.108642.

ACKNOWLEDGMENTS

We appreciate the effort of all clinical physicians and researchers who contributed to this work, as well as the understanding and support of the patients and their parents. This work was supported by Shenzhen Science and Technology Program (JCYJ20220531091605012), National Natural Science Foundation of China (82100377), Beijing Nova Program (Z211100002121046), and National High Level Hospital Clinical Research Funding (2023-GSP-RC-01, 2023-GSP-ZD-2).

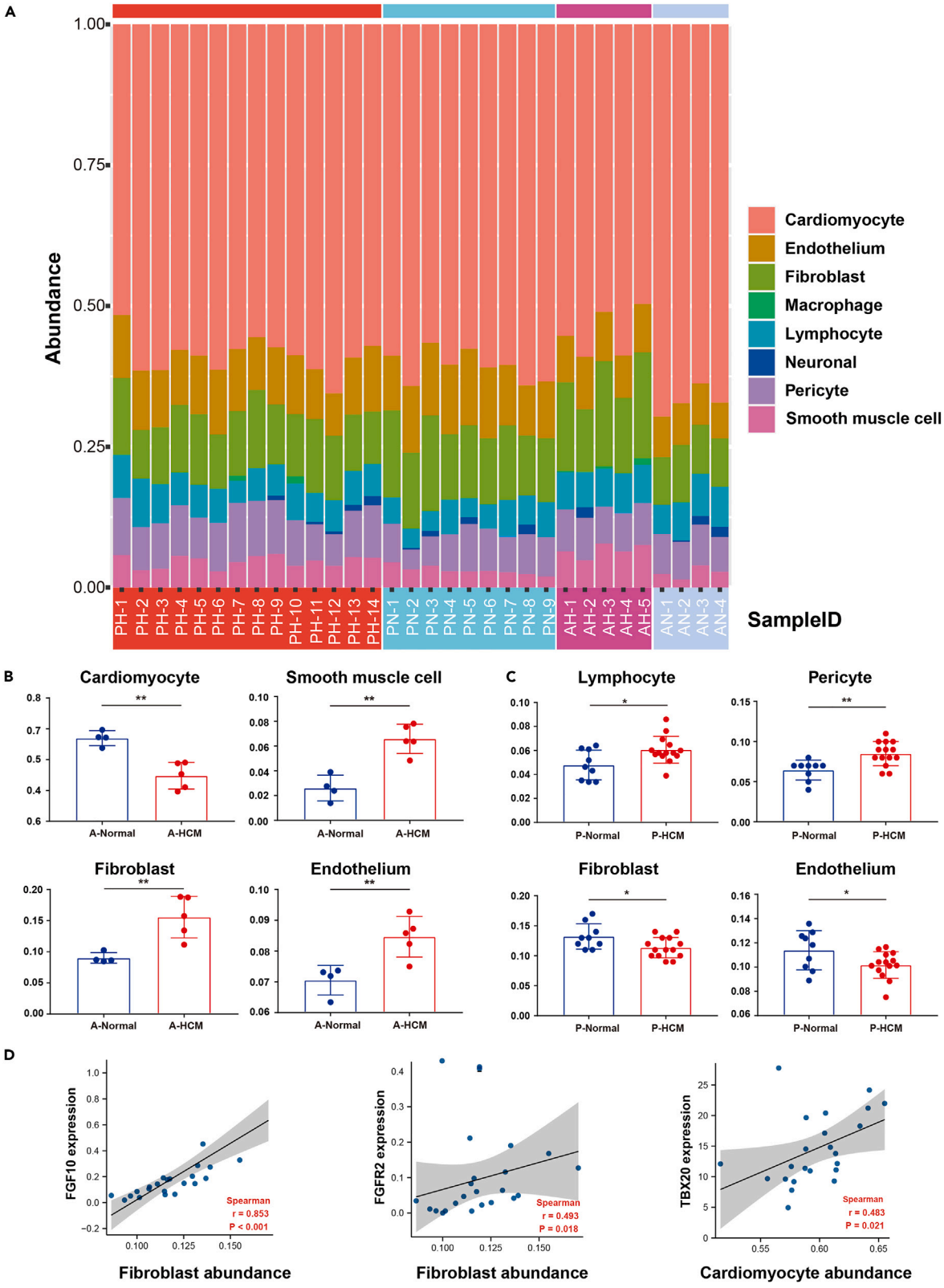
A
Abundance
1.00
0.75
0.50
0.25
0.00
PH-1 PH-2 PH-3 PH-4 PH-5 PH-6 PH-7 PH-8 PH-9 PH-10 PH-11 PH-12 PH-13 PH-14
PN-1 PN-2 PN-3 PN-4 PN-5 PN-6 PN-7 PN-8 PN-9
AH-1 AH-2 AH-3 AH-4 AH-5
AN-1 AN-2 AN-3 AN-4
SampleID
Cardiomyocyte
Endothelium
Fibroblast
Macrophage
Lymphocyte
Neuronal
Pericyte
Smooth muscle cell
B
Cardiomyocyte
Smooth muscle cell
Fibroblast
Endothelium
A-Normal
A-HCM
C
Lymphocyte
Pericyte
Fibroblast
Endothelium
P-Normal
P-HCM
D
FGF10 expression
Fibroblast abundance
Spearman
r = 0.853
P < 0.001
FGFR2 expression
Fibroblast abundance
Spearman
r = 0.493
P = 0.018
TBX20 expression
Cardiomyocyte abundance
Spearman
r = 0.483
P = 0.021

Figure 6. Deconvolution analysis of HCM and healthy donor transcriptomes in children and adults

(A) The histogram demonstrated deconvolution result of our bulk RNA sequencing data. Different types of cell abundance include cardiomyocytes, endothelial cells, fibroblasts, macrophages, lymphocytes, neurons, pericytes, and smooth muscle cells in each patient were shown.

(B) Changes in the abundance of different cell types in the A-HCM and A-Normal groups. Cardiomyocytes were significantly decreased while smooth muscle cell, fibroblast and endothelial cell fraction were significantly increased in A-HCM. The results are presented as the mean ± SEM. N = 4 in A-Normal group and n = 5 in A-HCM group. Differences between groups (p value) were calculated by unpaired two-tailed *t*-test. *p < 0.05; **p < 0.01; ***p < 0.001.

(C) Changes in the abundance of different cell types in the P-HCM and P-Normal groups. Fibroblasts and endothelial cell fraction were significantly decreased while lymphocytes and pericytes fraction were significantly increased in P-HCM. The results are presented as the mean ± SEM. N = 9 in P-Normal group and n = 14 in P-HCM group. Differences between groups (p value) were calculated by unpaired two-tailed *t*-test. *p < 0.05; **p < 0.01; ***p < 0.001.

(D) Spearman correlation analysis of the abundance of specific cell types (cardiomyocytes and fibroblasts) and the expression of *FGF10/FGFR2/TBX20*.

AUTHOR CONTRIBUTIONS

J.Z. and L.C. conceived the project. S.C. collected the heart samples and prepared sequencing libraries. S.C. and J.J.H. analyzed the transcriptomics data. Y.D.X. performed the validation experiments. S.C. wrote the manuscript with the input from all authors. Y.J., S.J.L., L.C. and J.Z. supervised the work.

DECLARATION OF INTERESTS

The authors declare no competing interests.

Received: April 10, 2023
Revised: October 22, 2023
Accepted: December 1, 2023
Published: December 5, 2023

REFERENCES

1. Nandi, D., Hayes, E.A., Wang, Y., and Jerrell, J.M. (2021). Epidemiology of Pediatric Hypertrophic Cardiomyopathy in a 10-Year Medicaid Cohort. Pediatr. Cardiol. *42*, 210–214.
2. Nugent, A.W., Daubeney, P.E.F., Chondros, P., Carlin, J.B., Cheung, M., Wilkinson, L.C., Davis, A.M., Kahler, S.G., Chow, C.W., Wilkinson, J.L., et al. (2003). The epidemiology of childhood cardiomyopathy in Australia. N. Engl. J. Med. *348*, 1639–1646.
3. Norrish, G., Kolt, G., Cervi, E., Field, E., Dady, K., Ziółkowska, L., Olivotto, I., Favilli, S., Passantino, S., Limongelli, G., et al. (2021). Clinical presentation and long-term outcomes of infantile hypertrophic cardiomyopathy: a European multicentre study. ESC Heart Fail. *8*, 5057–5067.
4. Arbelo, E., Protonotarios, A., Gimeno, J.R., Arbustini, E., Barriales-Villa, R., Basso, C., Bezzina, C.R., Biagini, E., Blom, N.A., de Boer, R.A., et al. (2023). 2023 ESC Guidelines for the management of cardiomyopathies. Eur. Heart J. *44*, 3503–3626.
5. Arola, A., Jokinen, E., Ruuskanen, O., Saraste, M., Pesonen, E., Kuusela, A.L., Tikanoja, T., Paavilainen, T., and Simell, O. (1997). Epidemiology of idiopathic cardiomyopathies in children and adolescents. A nationwide study in Finland. Am. J. Epidemiol. *146*, 385–393.
6. Anan, R., Shono, H., Kisanuki, A., Arima, S., Nakao, S., and Tanaka, H. (1998). Patients with familial hypertrophic cardiomyopathy caused by a Phe110Ile missense mutation in the cardiac troponin T gene have variable cardiac morphologies and a favorable prognosis. Circulation *98*, 391–397.
7. Axelsson Raja, A., Farhad, H., Valente, A.M., Couce, J.P., Jefferies, J.L., Bundgaard, H., Zahka, K., Lever, H., Murphy, A.M., Ashley, E., et al. (2018). Prevalence and Progression of Late Gadolinium Enhancement in Children and Adolescents With Hypertrophic Cardiomyopathy. Circulation *138*, 782–792.
8. Norrish, G., Ding, T., Field, E., Ziólkowska, L., Olivotto, I., Limongelli, G., Anastasakis, A., Weintraub, R., Biagini, E., Ragni, L., et al. (2019). Development of a Novel Risk Prediction Model for Sudden Cardiac Death in Childhood Hypertrophic Cardiomyopathy (HCM Risk-Kids). JAMA Cardiol. *4*, 918–927.
9. Ren, C.W., Liu, J.J., Li, J.H., Li, J.W., Dai, J., and Lai, Y.Q. (2016). RNA-seq profiling of mRNA associated with hypertrophic cardiomyopathy. Mol. Med. Rep. *14*, 5573–5586.
10. Pei, J., Schuldt, M., Nagyova, E., Gu, Z., El Bouhaddani, S., Yiangou, L., Jansen, M., Calis, J.J.A., Dorsch, L.M., Blok, C.S., et al. (2021). Multi-omics integration identifies key upstream regulators of pathomechanisms in hypertrophic cardiomyopathy due to truncating MYBPC3 mutations. Clin. Epigenetics *13*, 61.
11. Gao, J., Collyer, J., Wang, M., Sun, F., and Xu, F. (2020). Genetic Dissection of Hypertrophic Cardiomyopathy with Myocardial RNA-Seq. Int. J. Mol. Sci. *21*, 3040.
12. Maron, B.A., Wang, R.S., Shevtsov, S., Drakos, S.G., Arons, E., Wever-Pinzon, O., Huggins, G.S., Samokhin, A.O., Oldham, W.M., Aguib, Y., et al. (2021). Individualized interactomes for network-based precision medicine in hypertrophic cardiomyopathy with implications for other clinical pathophenotypes. Nat. Commun. *12*, 873.
13. Blackwood, E.A., Bilal, A.S., Stauffer, W.T., Arrieta, A., and Glembotski, C.C. (2020). Designing Novel Therapies to Mend Broken Hearts: ATF6 and Cardiac Proteostasis. Cells *9*.
14. Craig, R., Lee, K.H., Mun, J.Y., Torre, I., and Luther, P.K. (2014). Structure, sarcomeric organization, and thin filament binding of cardiac myosin-binding protein-C. Pflugers Arch. *466*, 425–431.
15. Viola, H.M., and Hool, L.C. (2019). Impaired calcium handling and mitochondrial metabolic dysfunction as early markers of hypertrophic cardiomyopathy. Arch. Biochem. Biophys. *665*, 166–174.
16. Santini, L., Coppini, R., and Cerbai, E. (2021). Ion Channel Impairment and Myofilament Ca(2+) Sensitization: Two Parallel Mechanisms Underlying Arrhythmogenesis in Hypertrophic Cardiomyopathy. Cells *10*.
17. Osterholt, M., Nguyen, T.D., Schwarzer, M., and Doenst, T. (2013). Alterations in mitochondrial function in cardiac hypertrophy and heart failure. Heart Fail. Rev. *18*, 645–656.
18. Ranjbarvaziri, S., Kooiker, K.B., Ellenberger, M., Fajardo, G., Zhao, M., Vander Roest, A.S., Woldeyes, R.A., Koyano, T.T., Fong, R., Ma, N., et al. (2021). Altered Cardiac Energetics and Mitochondrial Dysfunction in Hypertrophic Cardiomyopathy. Circulation *144*, 1714–1731.
19. Nollet, E.E., Duursma, I., Rozenbaum, A., Eggelbusch, M., Wüst, R.C.I., Schoonvelde, S.A.C., Michels, M., Jansen, M., van der Wel, N.N., Bedi, K.C., et al. (2023). Mitochondrial dysfunction in human hypertrophic cardiomyopathy is linked to cardiomyocyte architecture disruption and corrected by improving NADH-driven mitochondrial respiration. Eur. Heart J. *44*, 1170–1185.
20. Padula, S.L., Velayutham, N., and Yutzey, K.E. (2021). Transcriptional Regulation of Postnatal Cardiomyocyte Maturation and Regeneration. Int. J. Mol. Sci. *22*, 3288.
21. Piquereau, J., and Ventura-Clapier, R. (2018). Maturation of Cardiac Energy Metabolism During Perinatal Development. Front. Physiol. *9*, 959.
22. Li, F., Wang, X., Capasso, J.M., and Gerdes, A.M. (1996). Rapid transition of cardiac

myocytes from hyperplasia to hypertrophy during postnatal development. J. Mol. Cell. Cardiol. *28*, 1737–1746.

23. Zhang, J., Chang, J.Y.F., Huang, Y., Lin, X., Luo, Y., Schwartz, R.J., Martin, J.F., and Wang, F. (2010). The FGF-BMP signaling axis regulates outflow tract valve primordium formation by promoting cushion neural crest cell differentiation. Circ. Res. *107*, 1209–1219.
24. Vega-Hernández, M., Kovacs, A., De Langhe, S., and Ornitz, D.M. (2011). FGF10/FGFR2b signaling is essential for cardiac fibroblast development and growth of the myocardium. Development *138*, 3331–3340.
25. Urness, L.D., Bleyl, S.B., Wright, T.J., Moon, A.M., and Mansour, S.L. (2011). Redundant and dosage sensitive requirements for Fgf3 and Fgf10 in cardiovascular development. Dev. Biol. *356*, 383–397.
26. Sakabe, N.J., Aneas, I., Shen, T., Shokri, L., Park, S.Y., Bulyk, M.L., Evans, S.M., and Nobrega, M.A. (2012). Dual transcriptional activator and repressor roles of TBX20 regulate adult cardiac structure and function. Hum. Mol. Genet. *21*, 2194–2204.
27. Chakraborty, S., Sengupta, A., and Yutzey, K.E. (2013). Tbx20 promotes cardiomyocyte proliferation and persistence of fetal characteristics in adult mouse hearts. J. Mol. Cell. Cardiol. *62*, 203–213.
28. Marguerie, A., Bajolle, F., Zaffran, S., Brown, N.A., Dickson, C., Buckingham, M.E., and Kelly, R.G. (2006). Congenital heart defects in Fgfr2-IIIb and Fgf10 mutant mice. Cardiovasc. Res. *71*, 50–60.
29. Mahadevaiah, G., Gupta, M., and Ashwath, R. (2015). Down Syndrome with Complete Atrioventricular Septal Defect, Hypertrophic Cardiomyopathy, and Pulmonary Vein Stenosis. Tex. Heart Inst. J. *42*, 458–461.
30. Zheng, G.M., Bai, J., Tang, J.M., Zhu, F.C., and Jing, H.X. (2019). A case of hypertrophic cardiomyopathy combined with muscular ventricular septal defect and abnormal origin of right coronary artery. BMC Cardiovasc. Disord. *19*, 16.
31. Tikanoja, T., Jääskeläinen, P., Laakso, M., and Kuusisto, J. (1999). Simultaneous hypertrophic cardiomyopathy and ventricular septal defect in children. Am. J. Cardiol. *84*, 485–486.
32. Long, J., Huang, S., Bai, Y., Mao, J., Wang, A., Lin, Y., Yang, X., Wang, D., Lin, J., Bian, J., et al. (2021). Transcriptional landscape of cholangiocarcinoma revealed by weighted gene coexpression network analysis. Brief. Bioinform. *22*, bbaa224.
33. Langfelder, P., and Horvath, S. (2008). WGCNA: an R package for weighted correlation network analysis. BMC Bioinf. *9*, 559.
34. Kim, D., Paggi, J.M., Park, C., Bennett, C., and Salzberg, S.L. (2019). Graph-based genome alignment and genotyping with HISAT2 and HISAT-genotype. Nat. Biotechnol. *37*, 907–915.
35. Putri, G.H., Anders, S., Pyl, P.T., Pimanda, J.E., and Zanini, F. (2022). Analysing high-throughput sequencing data in Python with HTSeq 2.0. Bioinformatics *38*, 2943–2945.
36. Sidiropoulos, K., Viteri, G., Sevilla, C., Jupe, S., Webber, M., Orlic-Milacic, M., Jassal, B., May, B., Shamovsky, V., Duenas, C., et al. (2017). Reactome enhanced pathway visualization. Bioinformatics *33*, 3461–3467.
37. Newman, A.M., Steen, C.B., Liu, C.L., Gentles, A.J., Chaudhuri, A.A., Scherer, F., Khodadoust, M.S., Esfahani, M.S., Luca, B.A., Steiner, D., et al. (2019). Determining cell type abundance and expression from bulk tissues with digital cytometry. Nat. Biotechnol. *37*, 773–782.

STAR★METHODS

KEY RESOURCES TABLE

REAGENT or RESOURCE	SOURCE	IDENTIFIER
Antibodies		
FGFR2 Abcam #ab289968	Abcam	#ab289968
FGF10	ThermoFisher	#PA5-81501
GAPDH	Abcam	# ab8245
Biological samples		
Interventricular from P-HCM patients and health donors: see Table 1	This paper	N/A
Deposited data		
Raw bulk RNA-Seq data	This paper	https://github.com/JJHuJJ/Transcriptome-data-of-human-hypertrophic-cardiomyopathy.git
Oligonucleotides		
See Table S1 for qRT-PCR primer sequences	This paper	N/A
Software and algorithms		
ImageJ	National Institutes of Health, Bethesda, Maryland, USA	https://ImageJ.nih.gov/ij/
RStudio	Integrated Development for R. RStudio, Inc., Boston, Massachusetts, USA	http://www.rstudio.com/

RESOURCE AVAILABILITY

Lead contact

Further information and requests for resources and reagents should be directed to and will be fulfilled by the lead contact, Jing Zhang (zhangjingfw@163.com).

Materials availability

This study did not generate new unique reagents.

Data and code availability

- The bulk RNA-Seq data used and/or analyzed during the current study has been deposited at GitHub and are publicly available as of the date of publication. The accession link is listed in the key resources table. The raw RNA-Seq data of myocardium from A-HCM patients and healthy adults are available in the Gene Expression Omnibus database (GEO submission: GSE89714).
- This paper does not report original code.
- Any additional information required to reanalyze the data reported in this paper will be shared by the lead contact upon request.

EXPERIMENTAL MODEL AND STUDY PARTICIPANT DETAILS

Human subjects

Myocardial samples were collected from patients in our pediatric hypertrophic obstructive cardiomyopathy cohort who underwent surgical septal myectomy (8 male, 6 female). Normal control samples were collected from brain-dead infant donors (P-Normal) who died by accident or other diseases without heart malformation (6 male, 3 female). The echocardiogram data of cardiac function and anatomic structure were collected before death in P-Normal donors and before surgery in P-HCM patients. Donor hearts without dysfunction and malformation that were deemed not suitable for transplantation due to mismatching were enrolled in this study. The same region of left interventricular septal myocardial tissue from both P-HCM and P-Normal patients was collected by the same standard procedure. A total of fourteen P-HCM patients and nine healthy pediatric donors were enrolled for applying the following RNA-Seq procedure. Another four paired P-HCM and P-Normal samples were selected for qRT−PCR and Western blot validation experiments. All pediatric and adult HCM patients and healthy

donors were Chinese (Eastern Asians). Details of the age, sex and other clinical characteristics of P-HCM patients and healthy donors are listed in Table 1; details of identified gene mutations of P-HCM patients are listed in Table 2.

All patients were informed of every detail of this research and signed the informed consent form. All experiments were performed and approved by the ethics committee of Fuwai Hospital based on the Declaration of Helsinki.

METHOD DETAILS

Library preparation and RNA sequencing

RNA integrity was assessed using the RNA Nano 6000 Assay Kit of the Bioanalyzer 2100 system (Agilent Technologies, CA, USA). Briefly, mRNA was purified from total RNA using poly-T oligo-attached magnetic beads. Fragmentation was carried out using divalent cations under elevated temperature in First Strand Synthesis Reaction Buffer (5X). The library fragments were purified with the AMPure XP system (Beckman Coulter, Beverly, USA), and cDNA fragments of preferentially 370–420 bp in length were selected. PCR was performed with Phusion High-Fidelity DNA polymerase, universal PCR primers, and Index (X) Primer. Finally, PCR products were purified (AMPure XP system), and library quality was assessed on the Agilent Bioanalyzer 2100 system. The clustering of the index-coded samples was performed on a cBot Cluster Generation System using TruSeq PE Cluster Kit v3-cBot-HS (Illumina) according to the manufacturer's instructions. The library preparations were sequenced on an Illumina NovaSeq 6000 platform.

Quantitative real-time PCR (qRT–PCR)

Bulk tissue total RNA was extracted from 50 mg of frozen myocardial tissues using TRIzol (Invitrogen Inc., USA) and was measured by using a NanoDrop 2000 (Thermo Fisher Scientific). The qRT–PCR procedure was performed by using the SYBR PCR kit (Applied Biosystems, Foster City, CA) and QuantStudio 5 Real-Time PCR System (A28140, Applied Biosystems). The gene expression level was normalized to Rpl5 (human) within each sample using the relative $\triangle\triangle$CT method and is shown as a relative expression to control. The data presented are representative of at least three independent experiments. The details of the primer sequences in this study are listed in Table S1.

Western blot

RIPA lysis buffer (Beyotime, #P0013B) was used to lyse the frozen myocardial tissues. The target and reference proteins were separated by electrophoresis and then transferred to PVDF membranes. The membrane was blocked with blocking buffer (Beyotime, #P0023B) and then incubated with primary antibodies overnight at 4°C. The bands were detected by Chemiluminescent HRP Substrate (Millipore, USA), and *ImageJ* software was applied to measure the intensity of the bands.

QUANTIFICATION AND STATISTICAL ANALYSIS

Transcriptomics data analysis

WGCNA

WGCNA is a systems biology method used to describe gene association patterns between different samples.[32] Associations between identified candidate biomarker genes or therapeutic targets were assessed. Compared with only focusing on differentially expressed genes, WGCNA uses the information of thousands or nearly ten thousand genes with the greatest variation or all genes to identify gene sets of interest and perform significant association analysis with phenotypes. This analytical approach aims to find co-expressed gene modules and explore associations between gene networks and phenotypes of interest, as well as core genes in the network. The input data were differentially expressed genes, and weighted coefficient β values were used to screen and identify gene co-expression modules associated with the phenotypic feature. Analysis was performed using the R toolkit developed by Langfelder P et al.[33]

DEGs and gene ontology (GO) analysis

The NGS sequencing data of children and adults were aligned to the reference genome GRCh38.p13 using HISAT2 software by the same parameters,[34] and then HTSeq2 based on the Gene annotation file was used to calculate the expression level and perform gene annotation (GRCh38.104 http://ftp.ensembl.org/pub/release-104/gtf/homo_sapiens/Homo_sapiens.GRCh38.104.gtf.gz).[35] Then, DESeq2 was used to analyze the differentially expressed genes between the adult case group and the control group and the differentially expressed genes between the pediatric case group and the control group, and logFC>0.5 (upregulated) or logFC<−0.5 (downregulated) and q value < 0.05 were used to select significantly differentially expressed genes. Finally, the significantly differentially expressed genes between the adult group and the pediatric group were obtained. DEGs were interpreted by using the R package of the GO enrichment strategy.

Reactome pathway analysis

ReactomePA software was used for Reactome pathway analysis. ReactomePA is an R/Bioconductor package that provides enrichment analyses, including hypergeometric tests and gene set enrichment analyses.[36] A functional analysis can be applied to the genomic coordination obtained from a sequencing experiment to analyze the functional significance of genomic loci, including *cis*-regulatory elements and non-coding regions. A comparison among different experiments is also supported. Moreover, ReactomePA provides several visualization

functions to produce highly customizable, publication-quality figures. The source code and documents of ReactomePA are freely available through Bioconductor (http://www.bioconductor.org/packages/ReactomePA).

Deconvolution analysis

CIBERSORT is a deconvolution method for complex tissues, especially for human leukocyte subsets, based on linear support vector regression (SVR) from gene expression profiles. The abundance of cells was estimated based on gene expression data using a CIBERSORTx (https://cibersortx.stanford.edu/) analysis tool based on the Cibersort algorithm developed by Newman et al.[37] The cellular composition of the myocardial samples was inferred by deconvolution, where CIBERSORTx analysis was performed on the myocardial RNA-seq data with myocardial single nucleus RNA sequencing data as the reference.

Statistical analysis

Statistical analysis was performed with SPSS software version 21 (SPSS Inc., IBM Company, Chicago, Illinois, USA) and GraphPad Prism version 7 (GraphPad Software, La Jolla, CA, USA). Statistical details of the experiments (including number of cases, statistical tests and p value) and were provided in the figure legends.